Simulation Studies for The Future Balloon-Borne MeV Gamma-Ray Observatory: GRAMS
REU Program at Columbia University - Nevis Labs

Nerea Real Nsi[1]

[1]University of California, Santa Cruz

August 15, 2026

NEVIS LABORATORIES
COLUMBIA UNIVERSITY

Abstract

The Gamma-Ray and AntiMatter Survey (GRAMS) is a proposed balloon-borne experiment designed to study astrophysical gamma rays in the poorly explored MeV energy range and to search for signatures of cosmic antimatter. GRAMS will use a liquid argon time projection chamber (LArTPC) surrounded by scintillator detectors. Scintillation light produced in the liquid argon will provide a fast optical trigger, while the ionization charge will be used to reconstruct particle interactions.

This work uses the GRAMS simulation framework to characterize the atmospheric particle environment expected during the balloon flight planned Wanaka, New Zealand and to estimate the resulting detector and optical trigger rates. Atmospheric fluxes for photons, neutrons, protons, helium nuclei, muons, electrons, and positrons were generated using EXPACS/PARMA and converted into energy- and direction-dependent HEALPix maps. Monte Carlo particles sampled from these maps were propagated through a simulated GRAMS detector using Geant4, followed by simulations of the detector and optical readout response. The simulated event samples were normalized to physical rates in units of Hz.

Approximately 8.9 kHz of atmospheric particles were estimated to enter the detector, with approximately 4.1 kHz producing at least one energy deposition in the active liquid argon. Photons were found to be the largest contributor to detector occupancy. The optical trigger rate was also evaluated as a function of the summed, baseline-subtracted ADC threshold. Increasing the threshold substantially reduced the atmospheric trigger rate, but also introduced the possibility of rejecting lower-amplitude gamma-ray signals. A preliminary simulation of a Crab-like gamma-ray source was performed as a first step toward evaluating this trade-off. These results provide estimates of the background and data rates expected by the GRAMS readout electronics and support future optimization of the optical trigger threshold.

Contents

1 Introduction

1.1 The MeV Gamma-Ray Gap

Gamma rays provide a direct probe of some of the most energetic processes in the universe. Observations in the gamma-ray band can be used to study compact objects, supernovae, active galactic nuclei, gamma-ray bursts, and the electromagnetic counterparts of gravitational-wave and neutrino events. Gamma-ray spectral lines also provide information about nuclear reactions, radioactive decay, and the production of elements in astrophysical environments[1, 2].

Despite its scientific importance, the energy range between approximately 0.1 and 100 MeV remains less thoroughly explored than neighboring X-ray and high-energy gamma-ray bands. This region is often referred to as the "MeV gap." [1] One reason for the reduced sensitivity is that Compton scattering becomes an important photon interaction process in this energy range. A Compton interaction produces both a recoil electron and a scattered photon, and the incident direction cannot generally be reconstructed from a single measured interaction point. Instruments must therefore identify multiple interaction sites with sufficient spatial and energy resolution to reconstruct the incident gamma ray [1] .

Figure 1 shows the sensitivity of past, current, and proposed high-energy observatories as a function of photon energy. Compared with the neighboring X-ray and GeV gamma-ray bands, the MeV region has historically had lower instrumental sensitivity.

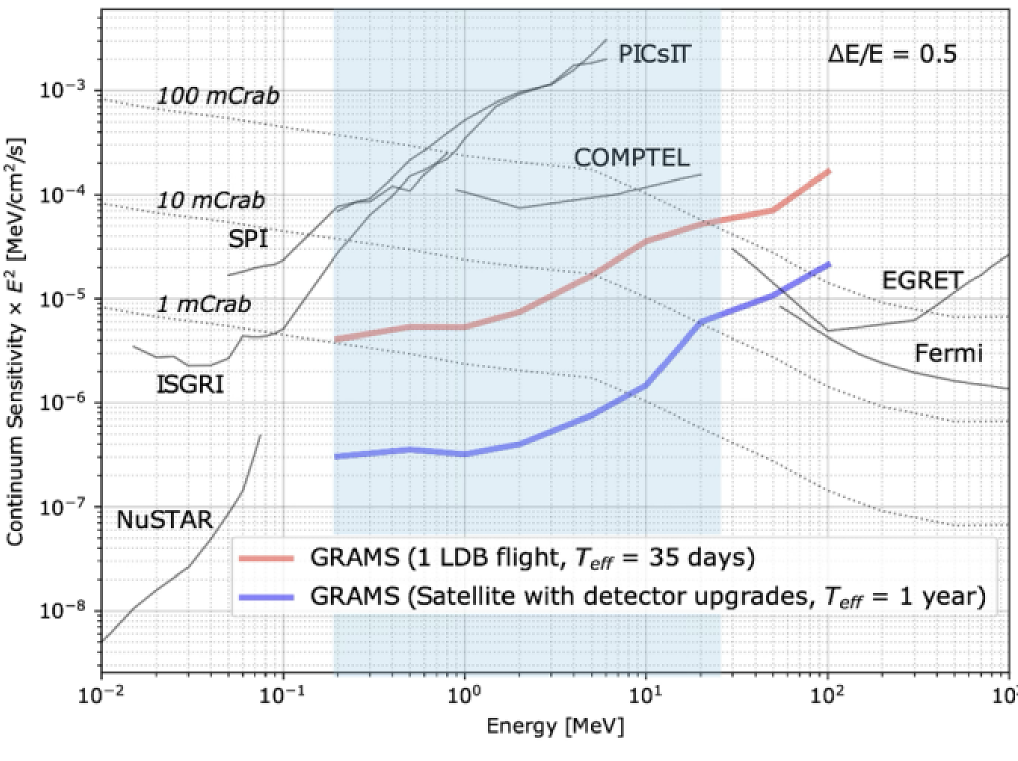

Figure 1: *Sensitivity of past, current, and proposed high-energy observatories as a function of photon energy. The shaded region indicates the approximate location of the MeV sensitivity gap that GRAMS is designed to address. Reproduced from Zeng et al. [2].*

1.2 The GRAMS Mission

The Gamma-Ray and AntiMatter Survey (GRAMS) is a proposed balloon-borne experiment designed to address two complementary scientific goals. The first is to improve sensitivity to astrophysical gamma rays in the MeV energy range. The second is to search for low-energy cosmic antimatter, including antideuterons, which may provide an indirect signature of dark matter[1, 2].

GRAMS will use a liquid argon time projection chamber (LArTPC), a detector in which charged particles ionize liquid argon as they pass through it. The resulting ionization electrons are drifted by an electric field toward readout electrodes, allowing the particle's energy deposition and three-dimensional trajectory to be reconstructed. The LArTPC serves as both a gamma-ray telescope and a particle detector. The current prototype stage, referred to as pGRAMS, is intended to demonstrate the detector, reconstruction, and readout technologies during flight operation required for a future larger-scale mission. Understanding the rates produced by atmospheric particles is particularly important for the design of the balloon-flight electronics.

The GRAMS development program includes prototype balloon flights followed by several balloon science flights and utlimately a satellite flight with increasingly larger LArTPC detector sizes. The current stage pGRAMS prototype represents an important step toward demonstrating liquid-argon detector operation, Compton-event reconstruction, and the associated readout systems in a balloon-flight environment.

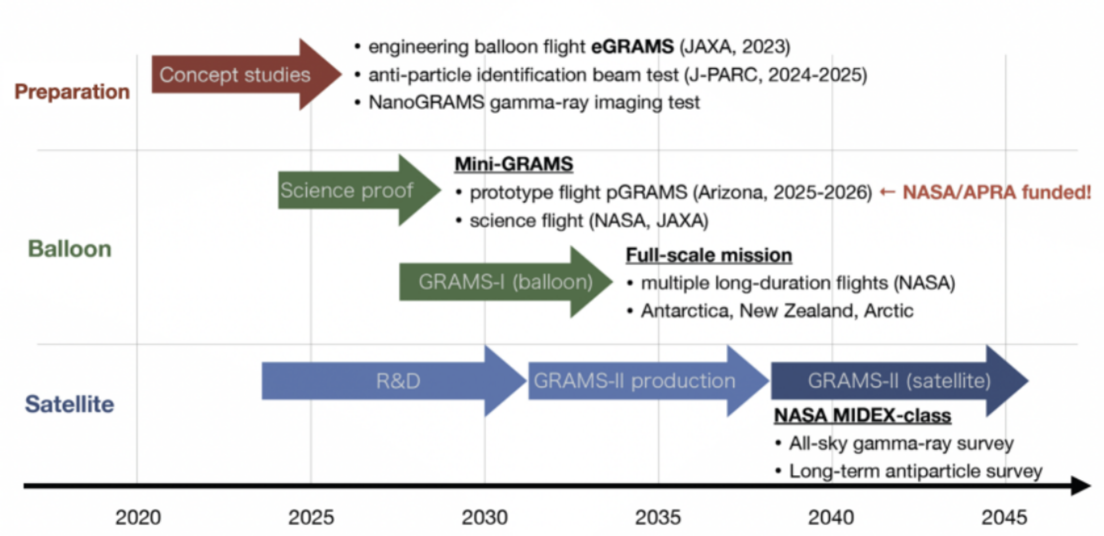

Figure 2: *Proposed development timeline for the GRAMS program, beginning with prototype detector studies and balloon flights and progressing toward larger-scale balloon and satellite missions. The present work contributes to the development of the optical readout and trigger system for the first GRAMS science-flight detector.*

1.3 The Liquid Argon Time Projection Chamber and Optical Trigger

When a particle deposits energy in liquid argon, it produces both ionization electrons and prompt scintillation light. The ionization electrons drift through the liquid argon under an applied electric field toward the anode, where their charge is measured[3]. Combining the charge distribution with the electron drift time allows the three-dimensional positions and deposited energies of particle interactions to be reconstructed.

The scintillation light is detected by silicon photomultipliers (SiPMs)[3]. Because the optical signal is produced nearly immediately after an interaction, it provides a fast indication that an event has occurred. This signal is therefore used to form the detector trigger, while the slower charge signal provides the information required for detailed event reconstruction.

Figure 3 illustrates the primary components and signals of the GRAMS LArTPC. The detector records the prompt scintillation-light signal with the SiPM readout plane while the ionization electrons drift toward the charge-readout anode.

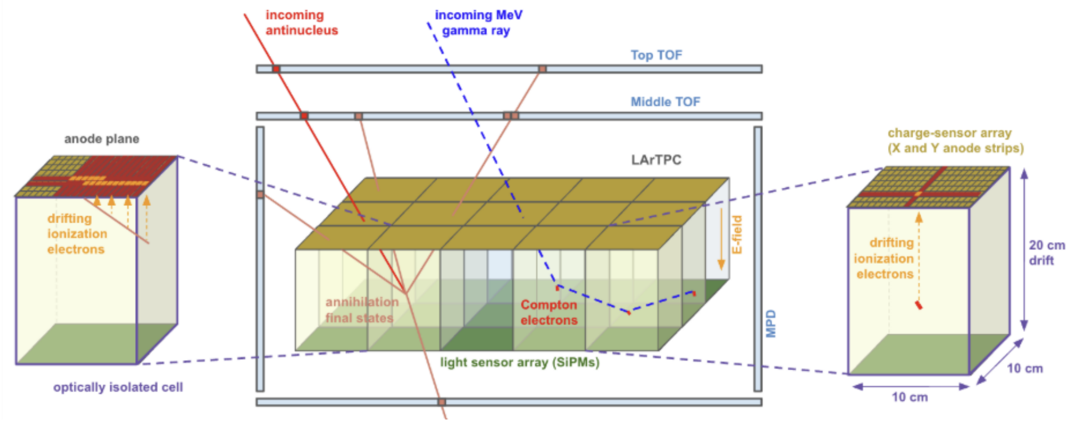

Figure 3: *Schematic of the GRAMS liquid argon time projection chamber. Particle interactions in the active liquid argon produce prompt scintillation light and ionization electrons. The light is detected by the SiPM readout plane and provides the fast optical trigger, while the ionization electrons drift toward the anode for charge readout and three-dimensional event reconstruction. Graphic adapted from the GRAMS Collaboration.*

At balloon altitude, the detector will be continuously exposed to atmospheric photons and charged particles. Many of these particles can deposit energy and produce scintillation light in the liquid argon. Recording the complete detector response for all particle-induced activity would require substantial storage and data-transfer bandwidth. A trigger is therefore required to identify candidate physical events and determine which portions of the detector data should be retained.

In the proposed optical readout, SiPM signals are digitized as analog-to-digital converter (ADC) waveforms. A region of interest (ROI) identifies a contiguous portion of a waveform containing a candidate scintillation pulse. A trigger may be issued when time-coincident ROIs from two or more neighboring SiPMs have a combined, baseline-subtracted amplitude above a selected threshold. A low threshold preserves smaller signals but produces a higher background and data rate. A high threshold reduces the background rate but may reject genuine low-energy gamma-ray events. The trigger threshold must therefore balance background suppression, signal efficiency, and the limitations of the readout electronics.

1.4 Project Objectives

The goal of this project is to characterize the atmospheric particle environment and optical trigger response expected for the GRAMS detector. The work is divided into the following four objectives.

1. Characterize the atmospheric particle environment. Atmospheric fluxes are modeled for the planned balloon-flight altitude and location. The simulated environment includes photons, neutrons, protons, helium nuclei, positive and negative muons, electrons, and positrons. Monte Carlo events are propagated through the simulated GRAMS detector and normalized to physical rates. This makes it possible to estimate how frequently atmospheric particles enter the detector, produce energy deposits in the active liquid argon, and generate optical signals.

2. Evaluate the atmospheric optical trigger rate. The optical trigger rate is calculated as a function of the the threshold applied to the combined, baseline-subtracted amplitude of coincident ROIs. This threshold scan is used to determine how strongly increasing it suppresses the atmospheric background and reduces the rate passed to the detector electronics, while keeping as much of the gamma-ray signal as possible.

3. Study the response to a Crab-like gamma-ray source. A simulated Crab-like gamma-ray sample is used to evaluate how the optical trigger efficiency changes under the same thresholds applied to the atmospheric background. This preliminary signal study provides a first step toward identifying a threshold that reduces background while preserving astrophysical gamma-ray events.

Together, these studies provide estimates of the particle, optical-response, and trigger rates that must be accommodated by the GRAMS readout electronics. They also establish the framework needed to guide the future selection of an optical trigger threshold.

2 Simulation Methodology

The atmospheric particle environment and detector response were modeled using a multi-stage simulation workflow. Atmospheric particle fluxes were first obtained from EXPACS/PARMA and converted into HEALPix maps describing the energy and arrival-direction distributions of each particle species. The GramsSky program sampled Monte Carlo primary particles from these maps, and GramsG4 propagated the particles through a Geant4 model of the GRAMS detector. Additional programs in the GRAMS simulation framework modeled the detector energy deposits, scintillation-light production, optical transport, silicon photomultiplier response, and digitized ADC waveforms.

2.1 Atmospheric Particle Fluxes

Atmospheric particle spectra and angular distributions were calculated using the EXPACS/PARMA [4, 5] model for the expected GRAMS science-flight environment. The atmospheric conditions used in this study corresponded to Wanaka, New Zealand, at an altitude of 30 km. The simulated primary particle species were photons, neutrons, protons, helium nuclei, positive and negative muons, electrons, and positrons.

The flux of each particle species was stored as a function of energy and arrival direction using HEALPix sky maps[6]. HEALPix divides the sphere into pixels of equal solid angle. Each energy layer of a map therefore contains the modeled particle flux associated with a particular energy interval and arrival direction. This representation preserves the directional structure of the atmospheric particle environment, including differences between particles arriving from above the detector and particles produced below or around it.

Figure 4 shows a representative atmospheric photon flux map used in the simulation.

For each atmospheric particle species, GramsSky [7] sampled $N_{\mathrm{MC}} = 10{,}000$ Monte Carlo primary particles from the corresponding HEALPix maps. Each Monte Carlo event represents one primary particle whose energy and arrival direction were randomly drawn from the modeled atmospheric distribution. The generated particles were then propagated through the detector geometry using GramsG4. Geant4[8] simulated the interactions of each primary particle and its secondary particles with the detector materials.

The number of generated Monte Carlo events is a computational choice and does not directly correspond to a physical observation time. In the simulation, each primary particle begins at $t = 0$, and there is no global elapsed time shared by the events. A normalization procedure was therefore required to determine the effective physical exposure represented by each simulated sample.

For each HEALPix pixel p, the particle flux was first integrated over the energy bins:

$$E_p = \sum_i \int_{E_i}^{E_{i+1}} \phi_{p,i}(E)\, dE, \tag{1}$$

where $\phi_{p,i}(E)$ is the differential particle flux in pixel p and energy interval i. The resulting quantity E_p has units of

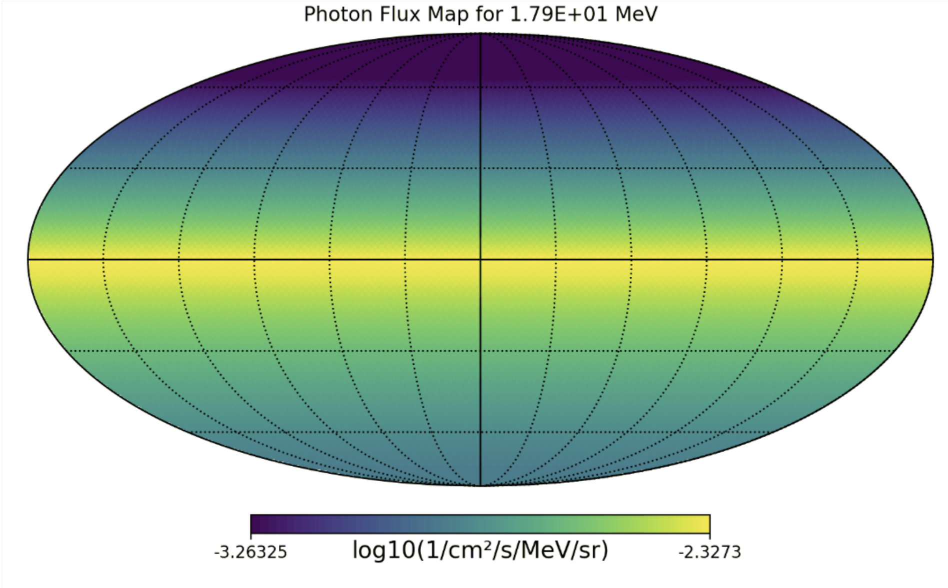

Figure 4: *Representative HEALPix map of the atmospheric photon flux calculated with EXPACS/PARMA for Wanaka, New Zealand, at an altitude of* 30 km*. The map encodes the modeled photon flux as a function of arrival direction for one energy interval.*

$$\mathrm{cm^{-2}\,s^{-1}\,sr^{-1}}. \tag{2}$$

The energy-integrated flux was then integrated over the solid angle of each pixel and summed across the sky:

$$S = \sum_p E_p \,\Delta\Omega_p, \tag{3}$$

where the solid angle of one HEALPix pixel is

$$\Delta\Omega_p = \frac{4\pi}{N_{\mathrm{pix}}} = \frac{4\pi}{12N_{\mathrm{side}}^2}. \tag{4}$$

The integrated quantity S has units of

$$\mathrm{cm^{-2}\,s^{-1}}. \tag{5}$$

The effective exposure represented by a sample containing N_{MC} simulated events was calculated as

$$T_{\mathrm{MC}} = \frac{N_{\mathrm{MC}}}{S}, \tag{6}$$

where T_{MC} has units of $\mathrm{cm^2\,s}$. Scaling a simulated counts distribution by T_{MC}^{-1} therefore converts the counts into a physical flux distribution:

$$\Phi_i = \frac{N_i}{T_{\mathrm{MC}}}, \tag{7}$$

where N_i is the number of simulated events in energy bin i.

The active liquid-argon volume used in this analysis had dimensions

$$30\ \mathrm{cm} \times 30\ \mathrm{cm} \times 20\ \mathrm{cm}. \tag{8}$$

The average detector cross section used in the rate normalization was calculated from the total surface area of the rectangular active volume:

$$A_{\text{TPC}} = \frac{2(xy + xz + yz)}{6}. \tag{9}$$

For the dimensions used in this study,

$$A_{\text{TPC}} = \frac{2\left[(30)(30) + (30)(20) + (30)(20)\right]}{6} = 700 \text{ cm}^2. \tag{10}$$

The physical rate associated with a selected category containing N_{selected} simulated events was then calculated as

$$R_{\text{selected}} = \frac{N_{\text{selected}}}{T_{\text{MC}}} A_{\text{TPC}}. \tag{11}$$

Figure 5 illustrates this normalization using the atmospheric photon sample. The original Monte Carlo counts distribution was first converted into a flux-weighted energy distribution using the effective exposure. The effective detector area was then applied to obtain the expected photon rate in each energy bin. The same procedure was performed separately for each atmospheric particle species.

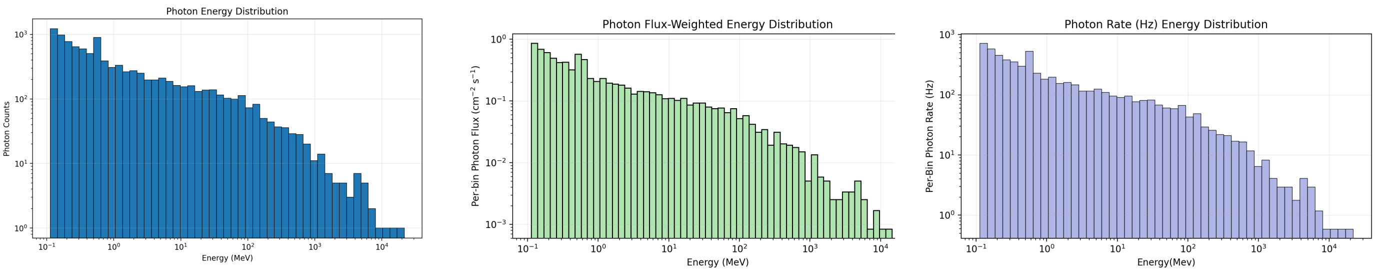

(a) *Monte Carlo counts.* ***(b)*** *Flux-weighted distribution.* ***(c)*** *Expected detector rate.*

Figure 5: *Conversion of simulated atmospheric photon counts into physical fluxes and detector rates.* ***(a)*** *Energy distribution of the* 10,000 *Monte Carlo photons sampled by* GRAMSSKY. ***(b)*** *Physical photon flux distribution obtained by scaling the Monte Carlo counts using the effective exposure derived from the HEALPix flux map.* ***(c)*** *Expected photon rate as a function of energy after applying the effective GRAMS detector area. This procedure was repeated for each simulated atmospheric particle species.*

2.2 Detector and Optical Response Simulation

The later stages of the GRAMS simulation chain converted the Geant4 energy depositions into simulated detector signals. When a particle deposits energy in the active liquid argon, it excites and ionizes argon atoms. Part of this energy is released as a prompt flash of scintillation light. The scintillation photons propagate through the active volume and may reach the silicon photomultipliers (SiPMs) located on the optical readout plane.

A SiPM is composed of many photosensitive microcells. When an incident scintillation photon is detected by a microcell, it initiates an electrical avalanche. The combined response of the SiPM microcells produces an analog electrical pulse whose amplitude is related to the amount of detected light. The readout electronics sample this signal at discrete times and convert the measured analog amplitude into digital analog-to-digital converter (ADC) counts. The resulting sequence of ADC values forms a digitized waveform.

The ADC waveforms used in this analysis were centered around a nominal baseline of 2048 ADC counts. In a physical readout system, samples fluctuate above and below the baseline because of electronics noise, dark counts, and other small variations in the detector and electronics response. Atmospheric particle activity may additionally produce real optical pulses throughout the flight. The present simulated samples did not include a complete model of electronics noise; however, the same baseline and threshold logic expected for the readout system was applied to the simulated waveforms.

A physical scintillation pulse appears as a temporary excursion of the waveform above its baseline. To distinguish candidate pulses from small baseline fluctuations, an individual-channel ADC threshold was applied. This first threshold is referred to as the region-of-interest threshold, or ROI threshold. A region of interest consists of a contiguous sequence of waveform samples associated with a candidate pulse that crosses the ROI threshold.

The ROI threshold used for the example shown in Figure 6 was 100 ADC counts above the nominal baseline:

$$A_{\text{ROI}} = 2048 + 100 = 2148 \text{ ADC counts.} \tag{12}$$

The peak amplitude of an ROI was measured relative to the baseline rather than using the raw ADC value:

$$A_{\text{peak}} = A_{\text{peak,raw}} - A_{\text{baseline}}. \tag{13}$$

The optical trigger required two ROIs from separate optical channels to occur within the same coincidence window. A coincidence requirement helps distinguish a detector-wide scintillation-light flash from a fluctuation observed in only one readout channel. For each pair of coincident ROIs, the two baseline-subtracted peak amplitudes were summed:

$$A_{\text{sum}} = A_{\text{peak},1} + A_{\text{peak},2}. \tag{14}$$

The summed amplitude was then compared with a second ADC threshold, referred to as the trigger threshold. An optical trigger was generated when

$$A_{\text{sum}} \geq A_{\text{th}}. \tag{15}$$

The ROI threshold and trigger threshold therefore perform two distinct tasks. The ROI threshold determines whether an individual waveform contains a candidate optical pulse, while the trigger threshold determines whether the combined coincident light signal is sufficiently large to initiate detector readout.

Figure 6 shows an example trigger candidate. The blue and orange curves are digitized ADC waveforms from two optical readout channels. They are not themselves the ROIs. The shaded regions indicate the ROIs selected around the coincident pulses. The green dashed line marks the nominal baseline of 2048 ADC counts, while the blue dashed line marks the ROI threshold at 100 ADC counts above baseline. The two baseline-subtracted peak amplitudes sum to 1743 ADC counts. Because this summed amplitude exceeds the preliminary trigger threshold of 1024 baseline-subtracted ADC counts, the event satisfies the optical trigger condition.

2.3 Trigger Threshold Study

A preliminary summed trigger threshold of 1024 baseline-subtracted ADC counts was used as a reference point. To study the dependence of the atmospheric trigger rate on this choice, the trigger threshold was varied over a wider range of ADC values. The ROI definition and coincidence requirement were held fixed while the summed trigger threshold was changed.

At each threshold A_{th}, the number of atmospheric events satisfying

$$A_{\text{sum}} \geq A_{\text{th}} \tag{16}$$

was counted separately for each simulated primary particle species. The fraction of incident events passing the optical trigger was calculated as

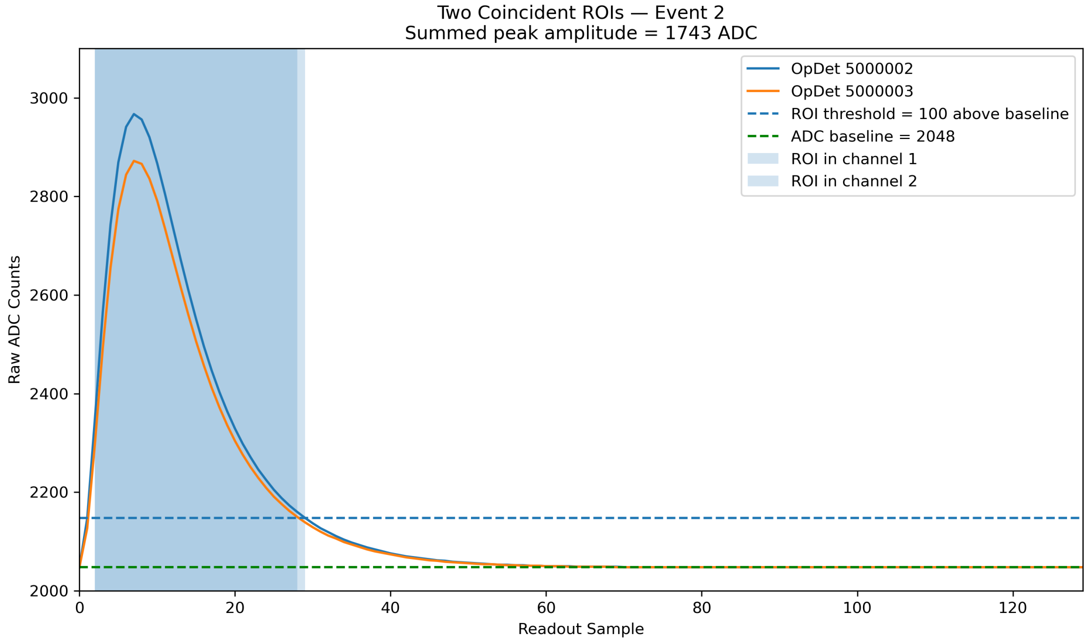

Figure 6: *Example optical trigger candidate containing two coincident SiPM pulses. The blue and orange curves show digitized ADC waveforms from two optical readout channels. The green dashed line indicates the nominal baseline of* 2048 *ADC counts, and the blue dashed line indicates the ROI threshold at* 100 *ADC counts above baseline. The shaded regions mark the ROIs selected around the coincident pulses. The two baseline-subtracted peak amplitudes sum to* 1743 *ADC counts, which exceeds the preliminary* 1024*-count trigger threshold and therefore produces an optical trigger.*

$$f_{\text{trig}}(A_{\text{th}}) = \frac{N\left(A_{\text{sum}} \geq A_{\text{th}}\right)}{N_{\text{incident}}}. \tag{17}$$

The corresponding physical trigger rate was then calculated using the normalized incident rate:

$$R_{\text{trig}}(A_{\text{th}}) = f_{\text{trig}}(A_{\text{th}})R_{\text{incident}}. \tag{18}$$

This threshold scan was used to quantify how increasingly restrictive summed ADC thresholds reduced the atmospheric event rate passed to the detector electronics. The resulting atmospheric trigger rates are presented in Section 3.

2.4 Preliminary Crab-Like Source Simulation

A preliminary astrophysical signal sample was generated using a power-law gamma-ray energy spectrum representative of the Crab Nebula. Unlike the atmospheric samples, which were generated from direction-dependent HEALPix flux maps, the Crab-like sample represented photons arriving from a localized astrophysical source.

The generated photons were propagated through the same Geant4 detector model used for the atmospheric particle samples. The resulting energy deposits were processed through the same detector-response, scintillation-light, optical transport, SiPM-response, and waveform-digitization stages. The same ROI selection, coincidence requirement, and summed ADC trigger condition were then applied to the Crab-like waveforms.

For each trigger threshold, the fraction of generated Crab-like events passing the optical trigger was calculated as

$$\epsilon_{\text{Crab}}(A_{\text{th}}) = \frac{N_{\text{Crab}}\left(A_{\text{sum}} \geq A_{\text{th}}\right)}{N_{\text{Crab,generated}}}. \tag{19}$$

At the current stage of this study, the Crab-like sample was used to evaluate the relative trigger efficiency as a function of threshold. Conversion of the surviving Monte Carlo events into a physical Crab source rate requires an additional normalization based on the assumed Crab flux, the photon-generation geometry, and the generated energy spectrum. The interaction-process distributions and preliminary threshold-dependent Crab-like counts are therefore presented as results in Section 3, rather than as part of the simulation methodology.

3 Results and Discussion

3.1 Atmospheric Background Composition

Table 1 summarizes the expected atmospheric particle, interaction, and optical-response rates at the detector. The total incident atmospheric particle rate was approximately 8.87 kHz. Of this incident population, approximately 4.14 kHz, or 46.7%, produced at least one energy deposition in the active liquid argon.

Photons produced the largest interaction rate, approximately 2.49 kHz, and were therefore the dominant contributor to the simulated liquid-argon occupancy. Although neutrons had the second-largest incident rate, only 46.6% produced a liquid-argon hit. In contrast, the simulated protons, helium nuclei, and muons had smaller incident rates but much larger interaction fractions.

Table 1: *Expected atmospheric particle, interaction, and optical-response rates. Rates were obtained from Monte Carlo samples normalized to the atmospheric flux. The* 1024*-count threshold refers to the summed, baseline-subtracted ADC trigger threshold. Electronics noise was not included.*

Particle	Incident rate (Hz)	Interacting rate (Hz)	Interaction fraction (%)	Nonzero ADC rate (Hz)	Rate $\geq$ 1024 (Hz)	Fraction $\geq$ 1024 (%)
Neutron	1719	801	46.6	720	476	27.7
Proton	501	433	86.4	432	430	85.8
Helium-4	35	35	99.4	35	35	99.2
μ^-	24	23	98.6	23	23	96.4
μ^+	19	19	98.8	19	19	98.4
Electron	419	178	42.4	176	161	38.1
Positron	246	183	74.7	183	168	68.3
Photon	5908	2494	42.2	2384	1898	30.6
Total	8870	4143	46.7	3971	3105	35.0

Approximately 3.97 kHz of the incident atmospheric event rate produced at least one nonzero simulated optical waveform. This corresponds to 44.8% of the total incident particle rate. The nonzero-ADC rate is close to the liquid-argon interaction rate, indicating that most simulated events that deposited energy in the active liquid argon also produced a detectable optical response in the noise-free simulation.

At the preliminary summed trigger threshold of 1024 baseline-subtracted ADC counts, the total atmospheric trigger rate was approximately 3.11 kHz. This corresponds to 35.0% of the total incident particle rate and approximately 78% of the nonzero-ADC rate. Atmospheric photons contributed approximately 1.90 kHz at this threshold and remained the largest component of the surviving trigger rate.

Because electronics noise was not included, the values in Table 1 represent only particle-induced optical activity. The total trigger rate of the physical detector may also contain contributions from SiPM dark counts, electronic fluctuations, and other readout effects.

3.2 Trigger Rate as a Function of ADC Threshold

Figure 7 shows the expected atmospheric trigger rate as a function of the summed, baseline-subtracted ADC threshold. For each particle species, the trigger rate decreased or remained constant as the threshold was increased. The total reduction was dominated by the photon and neutron components, which contained broad distributions of optical pulse amplitudes.

Atmospheric photons remained the dominant contribution across the threshold range. Their trigger rate decreased from approximately 2.4 kHz at the lowest thresholds to approximately 1.0 kHz near the upper end of the threshold scan. The neutron contribution also decreased substantially, while several charged-particle components changed more slowly over the same range.

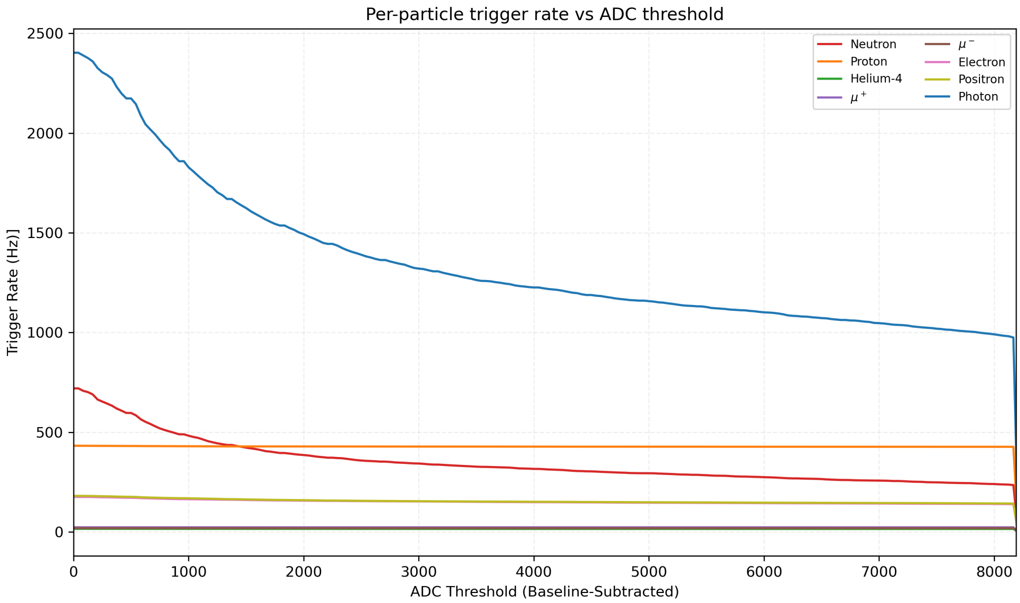

Figure 7: *Expected atmospheric optical trigger rate as a function of the summed, baseline-subtracted ADC threshold. Each curve shows the contribution from one simulated primary particle species. Increasing the threshold suppresses events with smaller optical amplitudes. Electronics noise was not included.*

The threshold scan demonstrates that the summed ADC threshold can regulate the rate of events passed to the detector readout. However, the atmospheric result alone does not determine an optimal operating threshold. A higher threshold reduces the background and expected data volume, but may also remove genuine gamma-ray events with smaller scintillation-light signals. The atmospheric trigger-rate curve must therefore be compared with the trigger efficiency of a representative astrophysical gamma-ray source.

3.3 Preliminary Crab-Like Source Results

The simulated Crab-like photon sample was first examined at the Geant4 stage to determine which primary photon interaction processes produced energy deposits in the active liquid argon. Figure 8 shows the number of events containing liquid-argon hits as a function of primary photon energy and interaction process.

As expected for MeV gamma rays, Compton scattering produced the largest number of liquid-argon hit events over much of the simulated energy range. Photoelectric absorption contributed mainly at lower energies, while pair production became increasingly important at higher energies. Photonuclear interactions were present but occurred much less frequently than the other simulated photon processes.

The Crab-like events were then processed through the detector-response and optical-trigger simulations. Figure 9 shows the raw number of simulated events passing the optical trigger as a

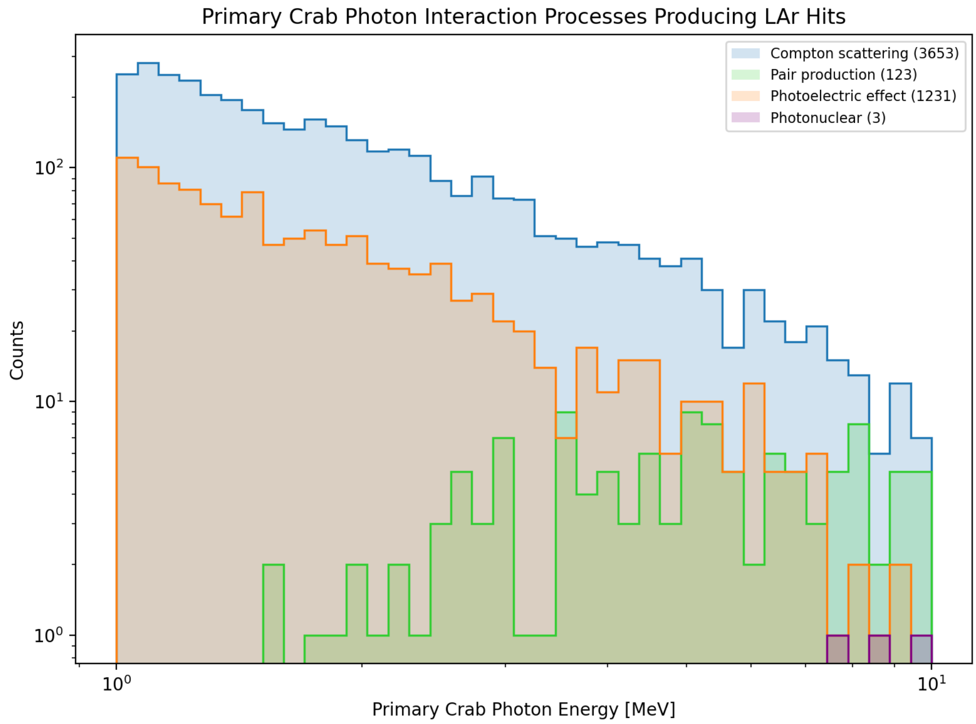

Figure 8: *Primary photon interaction processes associated with energy deposits in the active liquid argon for the simulated Crab-like source. The distributions are shown as a function of primary photon energy. Compton scattering, pair production, photoelectric absorption, and photonuclear interactions are displayed separately.*

function of the summed ADC threshold. The number of surviving events decreased continuously as the threshold was increased because progressively larger optical amplitudes were required to satisfy the trigger condition.

The declining distribution confirms that the simulated source sample can be processed through the same optical-trigger framework used for the atmospheric background. However, the vertical axis in Figure 9 contains raw Monte Carlo counts rather than a physical source rate. The result therefore describes only the relative loss of simulated Crab-like events as the threshold is increased.

A direct signal-to-background comparison is not yet possible because the Crab-like sample must first be normalized using the assumed physical Crab flux, the photon-generation area, the generated energy spectrum, and the corresponding effective exposure. These results should therefore be interpreted as a preliminary trigger-response study rather than a measurement of GRAMS source sensitivity.

4 Summary and Conclusions

4.1 Atmospheric Particle and Interaction Rates

This work developed and applied a multi-stage simulation workflow to estimate the atmospheric particle environment and optical trigger rates expected for the future GRAMS science flight. Atmospheric particle fluxes generated with EXPACS/PARMA were converted into direction- and energy-dependent HEALPix maps for Wanaka, New Zealand, at an altitude of 30 km. Monte Carlo particles sampled from these maps were propagated through a Geant4 model of the GRAMS detector, followed by simulations of the detector and optical response.

The total atmospheric particle rate entering the detector was estimated to be approximately 8.9 kHz. Approximately 4.1 kHz, or 47%, produced at least one energy deposition in the active

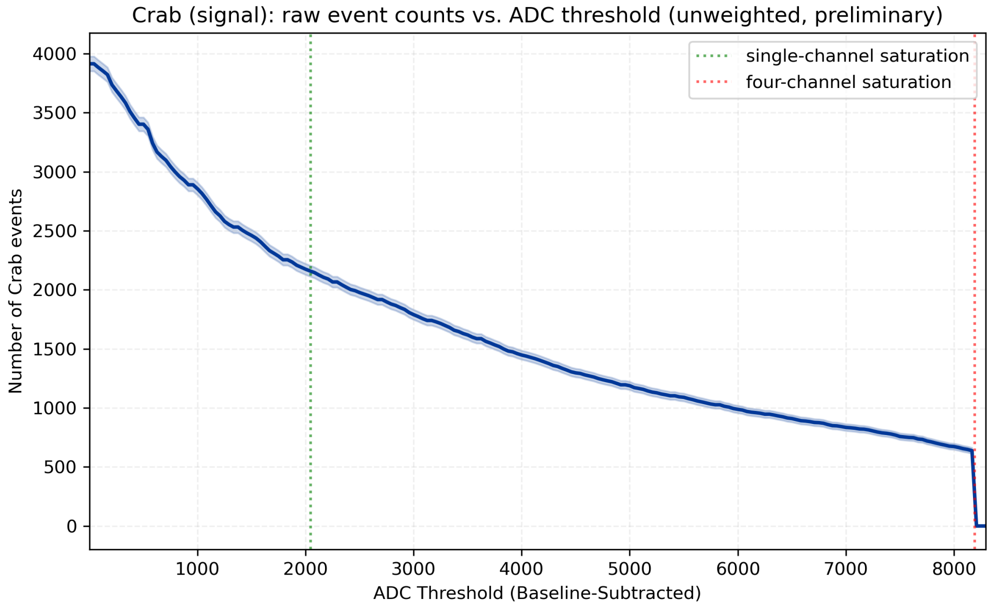

Figure 9: *Preliminary raw number of simulated Crab-like photon events passing the optical trigger as a function of the summed, baseline-subtracted ADC threshold. The vertical reference line indicates the preliminary* 1024*-count threshold. The counts have not been normalized to a physical Crab flux or observation time.*

liquid argon. Approximately 4.0 kHz also produced a nonzero optical waveform in the noise-free simulation.

Photons were the dominant contribution to both the liquid-argon interaction rate and the optical trigger rate. Although only approximately 42% of incident photons produced a liquid-argon hit, their large incident flux resulted in an interaction rate of approximately 2.5 kHz. This demonstrates that atmospheric photons are expected to be a major source of occupancy and optical activity during the GRAMS science flight.

The atmospheric background cannot be removed solely by identifying photon-like events, because both the desired astrophysical signal and a large component of the atmospheric background consist of gamma rays. The trigger must instead reduce the total event rate while preserving the subset of gamma-ray events that contain useful information for later reconstruction.

4.2 Trigger Threshold Trade-Off

At the preliminary summed threshold of 1024 baseline-subtracted ADC counts, the simulated atmospheric trigger rate was approximately 3.11 kHz, or 35% of the incident particle rate. Increasing the summed ADC threshold reduced the atmospheric trigger rate, demonstrating that the trigger threshold can be used to control the volume of data passed to the readout electronics.

The threshold scan also revealed the central trade-off in the trigger design. A higher threshold rejects a larger fraction of atmospheric events and reduces the required storage and bandwidth. However, it also rejects events with weaker scintillation-light signals. These may include lower-energy gamma rays, events with incomplete energy deposition, or interactions occurring in regions with reduced light collection.

Consequently, the lowest achievable background rate is not necessarily the optimal operating point. The desired threshold should instead provide an acceptable data rate while retaining a sufficiently large fraction of scientifically useful gamma-ray events. Determining this operating point requires comparing the atmospheric rate with the trigger efficiency of a representative astrophysical source.

4.3 Preliminary Crab-Like Source Study

The Crab-like photon simulation provides an initial source sample for evaluating this trade-off. The Geant4 interaction distributions showed that Compton scattering was a major source of energy deposits in the active liquid argon, consistent with the importance of Compton interactions for MeV gamma-ray detection. Pair production became more prominent at higher energies, while photoelectric absorption contributed primarily at lower energies.

The number of simulated Crab-like events passing the optical trigger decreased as the threshold was increased. This confirms that stronger atmospheric background rejection is accompanied by a loss of potential gamma-ray signal events. However, the current Crab-like distribution contains raw Monte Carlo counts and cannot yet be compared directly with the atmospheric rates in Hz.

The next required step is to normalize the Crab-like sample to its physical source flux and simulated generation geometry. Once this normalization is complete, the surviving Crab-like rate can be compared directly with the atmospheric trigger rate at each threshold. This comparison will allow the background reduction and signal retention to be evaluated on the same physical scale.

4.4 Limitations of the Current Study

Several limitations should be considered when interpreting the current results.

First, electronics noise was not included in the analyzed samples. The predicted nonzero-ADC and trigger rates therefore include only simulated particle-induced signals. Noise, SiPM dark counts, and other electronics effects may increase the rate of threshold crossings in the physical detector.

Second, the optical simulation and trigger logic represent the current detector and readout model. The channel grouping, coincidence timing, ROI definition, and ADC thresholds may change as the GRAMS electronics design is finalized.

Third, the Crab-like source sample has not yet been normalized to a physical source flux or exposure. The present Crab-like threshold distribution cannot be interpreted as an expected observed source rate or used to claim a source detection.

Finally, an event passing the optical trigger is not necessarily a scientifically useful Compton event. Successful gamma-ray reconstruction generally requires multiple resolvable interaction sites and sufficient deposited-energy information. Future studies should therefore determine how many triggered events also satisfy the requirements for Compton reconstruction.

4.5 Future Work

Future work will normalize the Crab-like simulation using the assumed source spectrum, physical Crab flux, and photon-generation geometry. The resulting source rate will then be compared with the atmospheric background rate as a function of ADC threshold.

The trigger study should also be extended to include realistic electronics noise and any updated channel-grouping or coincidence logic adopted for the GRAMS readout. In addition to counting triggered events, future analyses should identify events containing multiple liquid-argon interaction sites and determine the trigger efficiency specifically for reconstructable Compton events.

Together, these developments will support the selection of an optical trigger threshold that suppresses atmospheric activity to a manageable rate while preserving the MeV gamma-ray events required for the scientific goals of the future GRAMS science mission.

5 Acknowledgements

I would like to sincerely thank my mentors, Prof. Georgia Karagiorgi, Prof. Reshmi Mukherjee, Dr. William Seligman, Dr. Yinrui Liu, and Svanik Tandon for their guidance, mentorship, and support throughout this project. I would also like to thank Amy Garwood, the Nevis scientists, and the entire GRAMS Collaboration for creating a welcoming and supportive research environment. This summer has been an invaluable opportunity for my scientific and professional growth.

This material is based upon work supported by the National Science Foundation under Grant No. PHY-2349438.

References

[1] Tsuguo Aramaki, Per Ola Hansson Adrian, Georgia Karagiorgi, and Hirokazu Odaka. Dual MeV Gamma-Ray and Dark Matter Observatory—GRAMS Project. *Astroparticle Physics*, 114:107–114, 2020.

[2] J. Zeng et al. Gamma-Ray and AntiMatter Survey (GRAMS) Experiment, 2025. On behalf of the GRAMS Collaboration.

[3] Satoshi Takashima et al. Low-Noise SiPM Light Readout and ASIC-Based Charge Readout of a Liquid Argon Time Projection Chamber for MeV Gamma-Ray Measurements, 2026. arXiv:2607.11336.

[4] Tatsuhiko Sato. Analytical Model for Estimating Terrestrial Cosmic Ray Fluxes Nearly Anytime and Anywhere in the World: Extension of PARMA/EXPACS. *PLOS ONE*, 10(12):e0144679, 2015.

[5] Tatsuhiko Sato. Analytical Model for Estimating the Zenith Angle Dependence of Terrestrial Cosmic Ray Fluxes. *PLOS ONE*, 11(8):e0160390, 2016.

[6] Krzysztof M. Górski, Eric Hivon, Anthony J. Banday, Benjamin D. Wandelt, Frode K. Hansen, Martin Reinecke, and Matthias Bartelmann. HEALPix: A framework for high-resolution discretization and fast analysis of data distributed on the sphere. *The Astrophysical Journal*, 622(2):759–771, 2005.

[7] William Seligman. GramsSim: Simulation software for the GRAMS experiment. `https://codeberg.org/wgseligman/GramsSim`, 2026. Develop branch, accessed August 1, 2026.

[8] S. Agostinelli, J. Allison, K. Amako, J. Apostolakis, H. Araujo, P. Arce, et al. Geant4—a simulation toolkit. *Nuclear Instruments and Methods in Physics Research Section A: Accelerators, Spectrometers, Detectors and Associated Equipment*, 506(3):250–303, 2003.